

# Single Quantum Dot as an Optical Thermometer for Millikelvin Temperatures

Florian Haupt, Atac Imamoglu, and Martin Kroner\*

*Institute of Quantum Electronics, ETH Zürich, CH-8093 Zurich, Switzerland*

(Received 27 June 2014; published 1 August 2014)

Resonant laser spectroscopy of a negatively charged self-assembled quantum dot is utilized to measure the temperature of a three-dimensional fermionic reservoir down to 100 mK. With a magnetic field applied to the quantum dot, the single-charged ground state is split by the Zeeman energy. As the quantum dot is in tunnel contact with a thermal electron reservoir, a thermal occupation of the quantum-dot spin states is enforced by cotunneling processes. Resonant laser-induced fluorescence is used in order to measure the thermal quantum-dot spin-state population.

DOI: 10.1103/PhysRevApplied.2.024001

## I. INTRODUCTION

The work presented here is in the spirit of earlier work that uses the modification of the optical transition energy to extract information about the dynamics of the reservoirs that the quantum-dot (QD) electron interacts with [1–6]. Further, the atomlike electrical structure makes the QD an ideal probe for exploring the rich physics of higher-dimensional fermionic systems. In particular, when it comes to highly correlated electron states formed by a QD and a two-dimensional electron system such as the Kondo effect [7–9], the temperature of the electron system plays a major role, and low temperatures on the mK scale that can only be reached in a dilution refrigerator are desirable. While the electronic energy scale in a Fermi reservoir is determined by the temperature, the optical transitions of an isolated QD are hardly influenced by the temperature of the itinerant electrons or that of the lattice. The tight confinement (approximately equal to 30 meV) for the electron and hole wave function in the QD, which is much larger than the thermal energy at liquid helium temperatures (360  $\mu$ eV), leads to negligible thermal excitation. Furthermore, the QD-phonon interaction becomes only relevant for temperatures larger than 15 K, as the relevant phonon modes with sizable coupling strength become occupied [10,11]. Hence, the resonance linewidth of excitonic transitions in the QD is, in principle, limited only by the spontaneous emission rate [4]. This stands in stark contrast to transport spectroscopy of electrostatically defined QDs in a GaAs/AlGaAs two-dimensional electron system: there, the width of Coulomb blockade oscillations can be governed by the Fermi-Dirac distribution of electronic energies in the leads. Hence, transport spectroscopy provides a highly sensitive and direct way to measure the temperature of a fermionic reservoir in the mK range [12].

However, transport spectroscopy is not always applicable as a thermometer, in particular, for optical experiments.

In this paper, we present an all-optical approach to measure the temperature of a fermionic reservoir that is tunnel coupled to a QD. We perform resonant laser absorption spectroscopy on the single-charged exciton (trion) ground-state transitions of a single QD. In this way, we measure the thermal occupation of the QD ground state and obtain the temperature of the fermionic reservoir. We measure reproducibly a temperature of  $T \approx 130$  mK. Furthermore, this technique allows us to study the heating induced by laser fields.

## II. METHODOLOGY

### A. Experimental setup

The QD is embedded in a Schottky diode structure, which allows for a controlled charging of the QD with individual electrons [13–15]. To this end, the QD layer is separated by a 35-nm-thick tunnel barrier of intrinsic GaAs from a highly  $n$ -doped GaAs layer which acts as an electron reservoir. On top of the sample, a semitransparent metallic top gate is deposited in order to apply a voltage with respect to the electron reservoir. In order to obtain the optical spectrum of the QD, we scan a narrow-band laser across the trion transition of a single-electron charged QD and record the resonance fluorescence (RF) [16,17]. The magnitude of the RF signal measures the ability of the QD to resonantly scatter photons. The RF signal strength depends not only on the population of the ground state being addressed but also on the detuning of the laser from the resonance and the overlap between the laser polarization and the optical selection rules of the QD transition. The same objective lens is used to focus the excitation laser onto the sample and to collect the RF photons. This means that the RF signal would typically be overwhelmed by the laser light that is reflected from the sample. In order to suppress this laser background, we use cross-polarized excitation and detection [Fig. 1(a)]. This scheme requires that only the

\*Corresponding author.  
mkroner@phys.ethz.ch

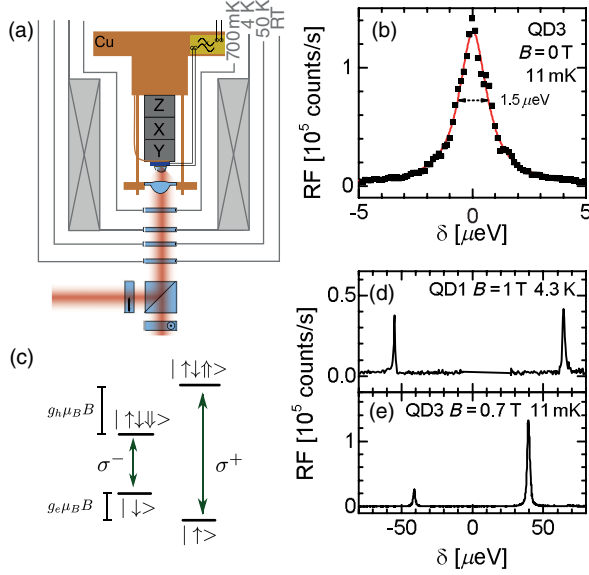


FIG. 1. (a) Schematic of the free-space optical dilution refrigerator. The sample is mounted on an XYZ-piezoelectric positioner and is in thermal contact with the Cu baseplate via thermal braids and the electrical connections. The radiation shields are labeled by their temperature. The vector magnet is mounted on the 4 K stage. Only the room temperature (RT) window is vacuum sealed. The optical excitation and collection are performed via a beam splitter. Two orthogonal polarizing filters are used for the RF experiment as described in the text. (b) Typical RF spectrum as a function of the laser detuning at mK temperature with no magnetic field applied. (c) Four-level scheme of the negatively charged QD with the relevant optical selection rules indicated. (d),(e) RF spectrum vs laser detuning at different magnetic fields and temperatures as labeled in the figures.

polarization component of the scattered light, which is perpendicular to the laser polarization, can be measured. Depending on the selection rules of the QD transitions, the basis of polarization for excitation and detection needs to be chosen carefully to obtain a good signal [16,17]. The collection efficiency is enhanced by a half-hemispherical ZrO<sub>2</sub> solid immersion lens (SIL) on top of the sample and a distributed Bragg reflector (28 layers) that has been grown below the QD layer (see Ref. [18] for details on the sample structure). A typical spectrum measured on a negatively charged QD with no magnetic field applied is shown in Fig. 1(b). We routinely observe a resonance linewidth  $\gamma \approx 1.5 \mu\text{eV}$ .

The sample is mounted in a cryogen-free dilution refrigerator (Bluefors LD250) with a base temperature of 7 mK. The base temperature is measured with a commercial RuO<sub>2</sub> thermometer (Lakeshore RX-102B) that is mounted directly on the mixing chamber flange. The readings of this thermometer will be regarded in the following as the base temperature of the cryostat ( $T_{\text{cryo}}$ ). The electron temperature of the sample, which is the subject of the presented measurement scheme, will be

simply labeled  $T$ . For free-space optical access to the sample, the cryostat is equipped with optical windows (fused silica) in all radiation shields of the different thermal stages [Fig. 1(a)]. For optimal transmission of the laser and RF photons, the windows are antireflection coated in the wavelength range  $\lambda = 600\text{--}1000$  nm. In order to suppress etaloning, the windows are wedged by 0.5°. With the windows installed, the base temperature of the cryostat increases to 11 mK due to the additional heat load, which is measured to be approximately equal to 1 μW. A single aspheric lens objective (numerical aperture, NA = 0.68) is used to focus the laser onto the sample surface and collect the backscattered photons that are ported out of the cryostat to be analyzed at room temperature. The sample is mounted on a piezoelectric-driven positioner stage [Attocube ANPx101/res (2×), ANPz101/res (1×)] with a resistive position readout. The resistive readout, however, induces significant heating and is switched off in order to reach the base temperature. To thermalize the sample, we connect it to the baseplate via thermal braids (Attocube ATC100). The signal cables for electrical contacting the sample are, for each line individually, thermalized by a second-order low-pass filter towards the grounded baseplate. The slip-stick mode of operation of the positioners requires connector cables with a large frequency bandwidth. Because of the significant capacitance of the piezoelectric actuators ( $C \approx 100$  nF) low-Ohmic wiring ideally below 2 Ω is necessary, and, hence, low-pass filtering as for the signal cables is not applicable. Superconductive wiring is used in order to minimize the heat load and to guarantee the functionality of the positioners at low temperatures. The cryostat is further equipped with a 9 T–3 T vector magnet.

## B. Temperature measurement

In order to measure the electron temperature of the back contact, we apply a magnetic field parallel to the optical excitation direction (Faraday geometry) which leads to a Zeeman splitting of the single-electron ground state of the QD [15,19]. Since the QD is tunnel coupled to the back contact, the occupation of the two electron-spin ground states will correspond to that of a thermal state. We obtain this ground-state population by measuring the trion transition RF signal, as described before. The two Zeeman-split ground states of the QD are connected by dipole-allowed optical transitions to the two Zeeman-split trion states. The two transitions differ in energy by  $\Delta E = (g_e + g_h)\mu_B B$ , and the optical selection rules are  $\sigma^+$  and  $\sigma^-$  polarized for the energetically higher and lower transitions, respectively, where  $g_e$  ( $g_h$ ) is the electron (hole)  $g$  factor, and  $\mu_B$  is the Bohr magneton [Fig. 1(c)]. In order to ensure the polarization independence of the measurement, we choose the laser to be linearly polarized, as in that case, the laser can drive both transitions with equal strength. Whether a certain transition is driven, and, hence, a corresponding

ground-state population is measured, can be controlled by setting the laser frequency to be resonant with one of the two transitions. A difference of the measured RF signal between the two transitions, in this case, can only stem from different ground-state population [20]. Further, the Rabi frequency  $\Omega$  is chosen to be small compared to the radiative emission rate of the QD trion. This corresponds to driving the trion transition below saturation in the so-called linear regime where the RF signal depends linearly on the laser power (or the square of the Rabi frequency) [21]. For small magnetic fields and high temperatures, the two electron spin states have equal population, and, consequently, the two resonances exhibit equal strength [Fig. 1(d)]. Here, the laser energy is swept in order to obtain the spectrum, which allows us to observe both transitions in the same trace. If the Zeeman splitting of the electron ground state exceeds the electron temperature of the back contact, the population of the two electron spin states ( $\rho_{\downarrow}, \rho_{\uparrow}$ ) will differ, resulting in different RF signal strengths as shown in Fig. 1(e). There, the temperature of the cryostat is  $T_{\text{cryo}} = 11$  mK, and the magnetic field is  $B = 0.7$  T. Because of the tunnel coupling of the QD electron states to the thermal electron system of the back contact, the ground-state populations  $\rho_{\downarrow}, \rho_{\uparrow}$  will approach a thermal distribution in steady state [20,22]. The thermal population  $\rho_{\downarrow}, \rho_{\uparrow}$  is given by the Fermi-Dirac distribution, and the relative amplitudes of the absorption resonances  $A_{\text{blue}}$  for the high-energy transition (corresponding to the spin-up ground state) and  $A_{\text{red}}$  for the low-energy transition (corresponding to the spin-down ground state) can be written as

$$\rho_{\downarrow}, \rho_{\uparrow} = \frac{A_{\text{red,blue}}}{A_{\text{red}} + A_{\text{blue}}} = \frac{1}{\exp(\pm \frac{g_e \mu_B B}{k_B T}) + 1}. \quad (1)$$

Here,  $k_B$  is the Boltzmann constant. The externally applied magnetic field is given by  $B$ , and the temperature of the Fermi sea of electrons in the back contact is  $T$ .

In Fig. 2(a),  $\rho_{\downarrow}, \rho_{\uparrow}$  are plotted for two different QDs (QD1, QD3) as a function of the magnetic field. By fitting Eq. (1) to the data points, we obtain the temperatures  $T$  as labeled in the plot. The electronic  $g$  factors of the QDs ( $g_{e,\text{QD1}} = 0.61$ ,  $g_{e,\text{QD3}} = 0.59$ ) are determined by a two-laser repump experiment as described in Ref. [23]. As a comparison, the inset in Fig. 2(a) shows  $\rho_{\downarrow}, \rho_{\uparrow}$  when the sample is cooled only by the pulse tube cooler ( $T_{\text{cryo}} \approx 4$  K). Even at magnetic fields up to 8 T, the amplitude ratio is not changing appreciably at these temperatures, and, hence, the accuracy of this measurement is limited. For a base temperature of  $T_{\text{cryo}} = 11$  mK, we find the electron temperature of the sample to be  $T \approx (130 \pm 7)$  mK with a very high accuracy of 5% (integration time per point  $t_c = 20$  ms). However, the measured electron temperature of the samples is more than 1 order of magnitude higher than the base temperature of the cryostat. For the given measurements, we find a shot noise limited [4] precision of the measurement scheme of 0.7% for an integration time of 1 s [24]. In order to obtain a value of the temperature, only the laser needs to be scanned while the gate voltage and magnetic field can be kept constant. Hence, the electrical bandwidth of the sample is not important for the performance of the scheme. Since the gate-voltage drifts in the sample are minimal, only the

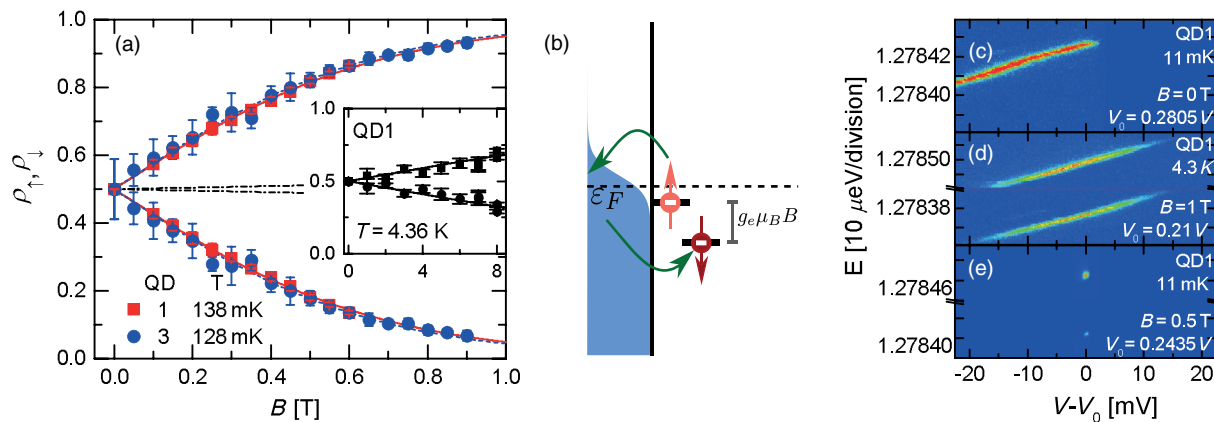


FIG. 2. (a) Relative RF amplitude of the two optical transitions [as shown in Figs. 1(d) and 2(e)] as a function of the magnetic field for two different QDs (red squares and blue dots). The correspondingly colored lines indicate the thermal occupation of the QD electronic spin states based on Eq. (1). The inset shows a similar measurement obtained only with the pulse tube cooling (also indicated by the dash-dotted line in the main figure). (b) Schematic to illustrate the cotunneling process. An electron from the QD (red arrow) can tunnel into the Fermi reservoir (occupation relative to the Fermi energy  $\epsilon_F$  indicated by the blue area) and replaced by another electron of opposite spin. The probability of the resulting spin-state occupation scales with the Zeeman splitting between the two states. (c)–(e) Color-coded RF counts [blue (low counts), red (high counts)] as a function of laser energy and gate voltage at the edge of the  $X^-$  plateau. All measurements are taken on QD1. The magnetic field and temperature are labeled and so is the gate-voltage offset  $V_0$  indicating the charging voltage for the second electron. This voltage varies over time and, hence, is different for these data sets that were taken over the course of several weeks.

mechanical stability of the optical setup limits the long-term stability of the measurement scheme [25]. The minimal electron temperature that can be measured this way is limited by the fluctuations of the Overhauser field generated by the nuclear spin ensemble of the QD to be  $T = 6$  mK [26].

### III. RESULTS AND DISCUSSION

#### A. Thermalization of the electron spin

Before discussing the implications of the unexpectedly high measured temperature, we explain the framework of the temperature measurement where several important points need to be considered for an accurate temperature estimate. As discussed before, the thermal occupation of the QD electronic states is imposed by the coupling to the thermal electron system of the back contact. In particular, a fast and efficient thermalization of the QD electron via cotunneling processes to the electron reservoir has to be guaranteed. At finite magnetic fields in the center of the voltage range of the stable single-electron state in the QD (the  $X^-$  plateau), the RF signal vanishes due to optical spin pumping and slow spin relaxation [27]. This is a consequence of the fact that both exchange with the Fermi sea and hyperfine flip-flop terms are suppressed [22]. However, if the QD electronic state is tuned close to the Fermi level, fast cotunneling [28] will lead to a thermal occupation of states in the QD, and the RF signal is restored. This is sketched in Fig. 2(b). In order to ensure a thermal state in the QD, we have to apply a gate voltage such that the measured resonance signal (of the two transitions combined) becomes similar to the signal measured with no magnetic field applied. In Figs. 2(c)–2(e), the RF counts are color coded as a function of laser energy and gate voltage for several temperatures and magnetic fields. In Fig. 2(c), the end of the charge stability plateau of the singly charged QD is shown at  $B = 0$  T and  $T_{\text{cryo}} = 11$  mK. The RF amplitude is constant over the  $X^-$  plateau and then drops off when the QD ground state is doubly charged at more positive gate voltages. This abrupt drop of the RF signal resembles the sharp Fermi-Dirac distribution of the fermionic reservoir of electrons, which is the source for the second electron tunneling into the QD at this voltage. Here, the distribution of occupied states in the back contact is probed by the electron state of the QD whose energy relative to the Fermi energy is given by the electrostatic energy,  $E_{\text{el}} = eV_g/\eta$  with the gate voltage  $V_g$  and the lever arm  $\eta = 5$  [29]. We observe an uncertainty of the electrostatic energy due to charge fluctuations in the vicinity of the QD [20,30] corresponding to an effective gate-voltage uncertainty of 0.5 mV. This limits a temperature-measurement scheme that is based on simply probing the occupation of states of the thermal reservoir with a QD electron level [26]. For our sample, this limit is on the order of 1 K. However, measuring the thermal occupation

of two Zeeman-split electron states is not sensitive to charge fluctuations, to first order. We require only the cotunneling rate to exceed a threshold value determined by the incident laser intensity. Therefore, we can measure an electron temperature that lies below the energy resolution given by the charge fluctuations in the sample. In Fig. 2(d), the cotunneling regime is plotted at  $B = 1$  T and  $T_{\text{cryo}} = 4.3$  K. The rather smooth decay of the signal strength towards the edges of the cotunneling regime is due to the large temperature as discussed before. Also, the amplitudes of the two resonances are almost equal at this low magnetic field. When the same experiment is repeated at the base temperature [Fig. 2(e)], the effect of the lower temperature on the gate-voltage dependence of the RF signal is striking. For  $B = 0.5$  T and  $T_{\text{cryo}} = 11$  mK, the voltage range where we find the QD ground state in a thermal state is reduced to one optical linewidth (limited by the spectral fluctuations), and the blue, high-energy transition clearly shows a larger RF amplitude than the red, low-energy transition. The reason for the narrowing down of the gate-voltage range, where the optical spin pumping is frustrated by cotunneling, stems from the fact that cotunneling is an inelastic tunneling effect: The Zeeman energy of the electron spin in the QD has to be provided or absorbed by the thermal distribution of the electrons in the back contact [22,31]. In order to obtain a precise reading of the temperature, we perform a measurement as shown in Figs. 2(d) or 2(e) for each magnetic field. We postselect the spectra in the center of the cotunneling range leading to a mean value and a standard deviation [data points and error bars in Fig. 2(a)] for  $\rho_{\downarrow}, \rho_{\uparrow}$ .

#### B. Influence of the nuclear spin environment

An important prerequisite for the described analysis is that the resonance line shape is not distorted by other influences such as the nuclear spin environment via the dragging effect [32,33]. In order to circumvent dragging of the QD resonance, we scan the laser fast across the resonance so that the rather slow nuclear spin dynamics cannot follow [33]. More precisely, we scan the laser energy with a rate of approximately 100  $\mu\text{eV/s}$  and average over 10 to 20 scans to obtain one spectrum.

#### C. Laser induced heating effects

From a four-level master equation simulation including the cotunneling mechanism, we conclude that the influence of the resonant laser on the ground-state population is negligible for realistic parameters. To experimentally verify that fast and efficient spin pumping does not alter the temperature measurement, we also perform a measurement in Voigt rather than in Faraday geometry (data not shown). With an applied in-plane magnetic field, the spin-pumping rate is as fast as the radiative-decay rate [34] and about a factor of 200 faster than in Faraday geometry. Still, the temperature measurement results in similar values as

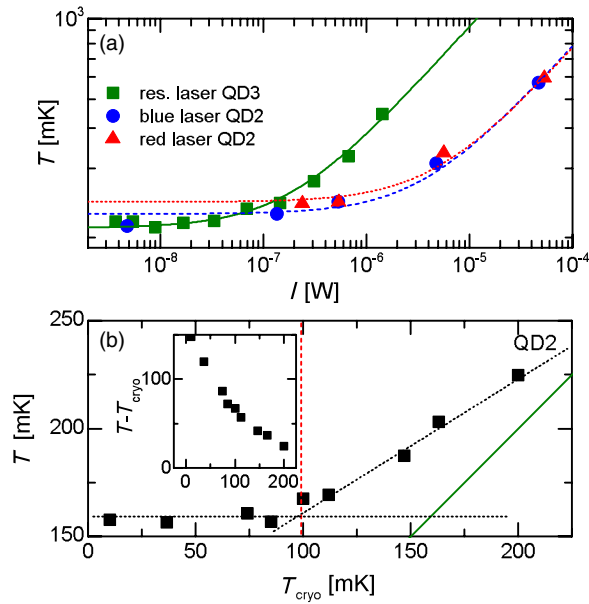


FIG. 3. (a) Measured temperature as a function of the incident laser power. The green squares stand for the experiment with increasing resonant probe laser power measured on QD3. The red and blue data points are acquired for a constant probe laser power ( $P = 100$  nW) for different red ( $\lambda_{\text{red}} = 980$  nm) or blue ( $\lambda_{\text{blue}} = 904$  nm) detuned heating lasers on QD2. The lines are guides to the eye. (b) Measured temperature  $T$  as a function of the mixing chamber temperature  $T_{\text{cryo}}$  (black squares). The dotted lines are guides to the eye; the green line indicates thermal equilibrium. The inset shows  $T - T_{\text{cryo}}$  vs  $T_{\text{cryo}}$ . This data set is obtained on QD2.

before. However, the laser power can certainly lead to local heating of the sample, in particular, due to a considerable absorption of the laser light by the metallic top gate. To exclude laser heating, we measure the sample temperature for different laser powers on QD3. In Fig. 3(a), the obtained temperature values are plotted as functions of the laser power measured outside the cryostat. We find that for laser powers below 50 nW, the measured temperature remains constant at a value of  $T = 130$  mK. Hence, we can exclude that the laser power is restricting the temperature measurement. For larger laser power, we do, indeed, observe an increase of the temperature hinting towards laser heating effects. In order to exclude distortion of the temperature measurement by saturation of the trion transition [21], we perform a control experiment with a second, off-resonant laser [35,36] (the two-laser experiment is performed on QD2.). While the resonant probe laser remains at a power of 100 nW, either a red ( $\lambda_{\text{red}} = 980$  nm) or blue ( $\lambda_{\text{red}} = 904$  nm) detuned laser is varied in power. The resulting temperature as a function of the off-resonant laser power is shown in Fig. 3(a) by the red and blue points, respectively. This procedure allows us to measure the local laser-induced heating and resulting temperature up to a laser power of  $50 \mu\text{W}$ , a power which is 2 orders of magnitude above the saturation power and also larger than

the cooling power of the dilution unit (approximately  $8 \mu\text{W}$ ) at base temperature. We observe that the heating due to the resonant laser is considerably larger than that due to the off-resonant laser, while the blue- and red-detuned lasers have a very similar heating effect. This is remarkable since the blue-detuned laser is very close to the excited QD states. Hence, we would have expected a stronger heating effect for the red-detuned laser which is farther away from most residual absorption transitions. Both lasers, however, lie beyond the bandwidth of the Bragg mirror in the sample. This means that the laser light will be transmitted through the sample and finally be absorbed on the sample holder which is very well thermalized. The resonant laser, however, will be reflected by the mirror and pass through the gate a second time where it can be absorbed again. This does not explain though the large difference between the resonant and the off-resonant laser heating effects which stems most probably from saturation effects. From the similar results for the two off-resonant lasers, we can conclude that the most important mechanism for laser-induced heating in these cases is the absorption by the metallic top-gate electrode.

The measurements at low-laser power indicate that the electron temperature is not limited by the heating effects of the measurement laser. The fact that the measured electron temperature is larger than the base temperature of the cryostat means that the heat generated in the sample via mechanisms other than the incident laser exceeds the cooling power of the cryostat at the sample due to imperfect thermal coupling of the sample to the baseplate. It has to be said that since the sample has to be movable and, hence, cannot be mounted in close proximity of the cold plate, it is not too surprising that a thermal gradient forms across the superstructure of the microscope. The cooling power mediated by the cables, the most significant cooling mechanism for the electron system in the sample at low temperatures, is limited despite the careful thermalization and electric filtering. To explore these limits, we measure the sample temperature for different base temperatures on QD2. The data are shown in Fig. 3(b). In order to ensure the independence of the individual measurements of this experiment, the data were taken in random order. For temperatures of the baseplate below 100 mK, the measured sample temperature  $T$  remains constant at 160 mK [37]. Above 100 mK, the sample temperature starts to increase and approaches the base temperature [indicated by the green line in Fig. 3(b)]. For clarity, the inset shows the difference between the sample and the baseplate temperature. Since the cooling power of the dilution unit depends strongly on temperature (quadratically at these low temperatures) for increasing temperature and, hence, increasing cooling power, the gradient that forms across the thermal anchoring of the sample diminishes from 150 mK at  $T_{\text{cryo}} = 11$  mK down to 25 mK at  $T_{\text{cryo}} = 200$  mK. To estimate the effect of a gate-voltage-dependent current, we

measure the temperature of the electron system of the back contact for two different voltage regimes at the two edges of the  $X^-$  charging plateau differing by 100 mV. For both measurements with different currents, we find the same electron temperatures (data not shown).

#### IV. OUTLOOK AND CONCLUSION

The setup we describe in this paper allows for free-space laser spectroscopy on a single QD at mK temperatures. In particular, the free-space optical access allows for a high degree of polarization control and, in turn, for measurement of the resonance fluorescence of a QD. This allows us not only to perform laser spectroscopy but also to measure the power spectrum of the resonantly scattered photons. It has been proposed that a single QD strongly tunnel coupled to an electron reservoir that exhibits Kondo correlations for weak optical excitations [7] exhibits a nonequilibrium quantum-correlated state in the strong optical-driving limit [38]. Such a state is expected to alter the power spectrum from the well-known Mollow triplet [39,40] to a two-peak structure with a characteristic power dependence. In order to explore the feasibility to reach a sample temperature lower than the energy scale of the Rabi energy as well as the Kondo temperature, we measure the Rabi energy of the laser from the power broadening as well as directly from the Mollow triplet. In the inset of Fig. 4, a typical energy-resolved resonance fluorescence measurement is shown as a function of the laser detuning of QD2. This way we determine the Rabi energy  $\hbar\Omega$  for a strongly driven QD transition as a function of laser power (red data points in Fig. 4). The black data points in Fig. 4 indicate the

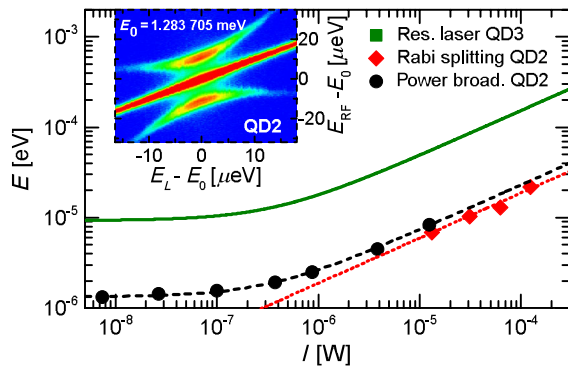


FIG. 4. Power broadening (black dots) of a resonantly driven QD transition and Rabi energy (red diamonds) of the resonant laser driving a QD vs the corresponding laser power. The dotted and dashed lines are guides to the eye. The green line represents the thermal energy measured as a function of laser power as shown in Fig. 3(b). The inset shows the color-coded QD emission as a function of the photon energy  $E_{RF}$  relative to the QD resonance energy  $E_0$  and the laser detuning from the resonance ( $E_L - E_0$ ). The data were obtained using a scanning Fabry-Perot spectral filter. The splitting at zero laser detuning gives the laser Rabi energy.

extracted linewidth from a resonant saturation experiment signifying power broadening [21]. In order to compare the energy scale of the Rabi energy with the temperature, we also plot the thermal energy corresponding to the laser-power-dependent temperature from Fig. 3(a). From this comparison, it is obvious that for any laser power, the Rabi energy is roughly 1 order of magnitude smaller than the thermal energy. In order to reach a situation where the Rabi energy can be comparable to the thermal energy of the electron reservoir, improvements need to be made to reduce the electron temperature and the laser-induced heating effects at high laser powers. To address the latter, the Schottky structure with the metallic top gate can be replaced by a pin-diode structure. Also, the light-matter interaction can be increased by replacing the  $ZrO_2$  SIL with one made from GaAs [41] or using spacial confinement of the light mode [42], which reduces the required laser power to obtain a certain Rabi energy. In order to further reduce the electron temperature, the sample structure can be optimized for a lower-resistance electrical connection to the Fermi reservoir.

In conclusion, we demonstrate an all-optical scheme to measure the electron temperature in a semiconductor down to the mK range. The present results open new ways for exploring the physics of semiconductor structures at ultra-low temperatures by high-resolution resonant optical spectroscopy. In particular, the ability to measure the resonance fluorescence gives direct access to the power spectrum of a single QD at mK temperatures in a cryogen-free dilution refrigerator.

We would like to acknowledge the work by Seilmeier *et al.* [43] that appeared recently.

#### ACKNOWLEDGMENTS

We thank Clemens Rössler, Khaled Karrai, and the Bluefors team for discussions and technical support.

- 
- [1] P. Maletinsky, A. Badolato, and A. Imamoglu, Dynamics of quantum dot nuclear spin polarization controlled by a single electron, *Phys. Rev. Lett.* **99**, 056804 (2007).
  - [2] E. A. Chekhovich, K. V. Kavokin, J. Puebla, A. B. Krysa, M. Hopkinson, A. D. Andreev, A. M. Sanchez, R. Beanland, M. S. Skolnick, and A. I. Tartakovskii, Structural analysis of strained quantum dots using nuclear magnetic resonance, *Nat. Nanotechnol.* **7**, 646 (2012).
  - [3] A. N. Vamivakas, Y. Zhao, S. Fält, A. Badolato, J. M. Taylor, and M. Atatüre, Nanoscale optical electrometer, *Phys. Rev. Lett.* **107**, 166802 (2011).
  - [4] A. V. Kuhlmann, J. Houel, A. Ludwig, L. Greuter, D. Reuter, A. D. Wieck, M. Poggio, and R. J. Warburton, Charge noise and spin noise in a semiconductor quantum device, *Nat. Phys.* **9**, 570 (2013).
  - [5] N. A. J. M. Kleemans, J. van Bree, A. O. Govorov, J. G. Keizer, G. J. Hamhuis, R. Nötzel, A. Yu. Silov, and P. M.

- Koenraad, Many-body exciton states in self-assembled quantum dots coupled to a Fermi sea, *Nat. Phys.* **6**, 534 (2010).
- [6] F. Haupt, S. Smolka, M. Hanl, W. Wüster, J. Miguel-Sanchez, A. Weichselbaum, J. von Delft, and A. Imamoglu, Nonequilibrium dynamics in an optical transition from a neutral quantum dot to a correlated many-body state, *Phys. Rev. B* **88**, 161304(R) (2013).
- [7] C. Latta, F. Haupt, M. Hanl, A. Weichselbaum, M. Claassen, W. Wüster, P. Fallahi, S. Fält, L. Glazman, J. von Delft, H. E. Türeci, and A. Imamoglu, Quantum quench of Kondo correlations in optical absorption, *Nature (London)* **474**, 627 (2011).
- [8] D. Goldhaber-Gordon, H. Shtrikman, D. Mahalu, D. Abusch-Magder, U. Meirav, and M. A. Kastner, Kondo effect in a single-electron transistor, *Nature (London)* **391**, 156 (1998).
- [9] S. M. Cronenwett, T. H. Oosterkamp, and L. P. Kouwenhoven, A tunable Kondo effect in quantum dots, *Science* **281**, 540 (1998).
- [10] M. Kroner, K. M. Weiss, S. Seidl, R. J. Warburton, A. Badolato, P. M. Petroff, and K. Karrai, Temperature dependent high resolution resonant spectroscopy on a charged quantum dot, *Phys. Status Solidi B* **246**, 795 (2009).
- [11] P. Borri, W. Langbein, S. Schneider, U. Woggon, R. L. Sellin, D. Ouyang, and D. Bimberg, Ultralong dephasing time in InGaAs quantum dots, *Phys. Rev. Lett.* **87**, 157401 (2001).
- [12] J. P. Pekola, K. P. Hirvi, J. P. Kauppinen, and M. A. Paalanen, Thermometry by arrays of tunnel junctions, *Phys. Rev. Lett.* **73**, 2903 (1994).
- [13] H. Drexler, D. Leonard, W. Hansen, J. P. Kotthaus, and P. M. Petroff, Spectroscopy of quantum levels in charge-tunable InGaAs quantum dots, *Phys. Rev. Lett.* **73**, 2252 (1994).
- [14] R. J. Warburton, C. Schäfflein, D. Haft, F. Bickel, A. Lorke, K. Karrai, J. M. Garcia, W. Schoenfeld, and P. M. Petroff, Optical emission from a charge-tunable quantum ring, *Nature (London)* **405**, 926 (2000).
- [15] A. Högele, S. Seidl, M. Kroner, K. Karrai, R. J. Warburton, B. D. Gerardot, and P. M. Petroff, Voltage-controlled optics of a quantum dot, *Phys. Rev. Lett.* **93**, 217401 (2004).
- [16] A. N. Vamivakas, Y. Zhao, C. Y. Lu, and M. Atatüre, Spin-resolved quantum-dot resonance fluorescence, *Nat. Phys.* **5**, 198 (2009).
- [17] P. Fallahi, S. T. Yilmaz, and A. Imamoglu, Measurement of a heavy-hole hyperfine interaction in InGaAs quantum dots using resonance fluorescence, *Phys. Rev. Lett.* **105**, 257402 (2010).
- [18] W. B. Gao, P. Fallahi, E. Togan, J. Miguel-Sanchez, and A. Imamoglu, Observation of entanglement between a quantum dot spin and a single photon, *Nature (London)* **491**, 426 (2012).
- [19] M. Bayer, G. Ortner, O. Stern, A. Kuther, A. A. Gorbunov, A. Forchel, P. Hawrylak, S. Fafard, K. Hinzer, T. L. Reinecke, S. N. Walck, J. P. Reithmaier, F. Klopff, and F. Schäfer, Fine structure of neutral and charged excitons in self-assembled In(Ga)As/(Al)GaAs quantum dots, *Phys. Rev. B* **65**, 195315 (2002).
- [20] A. Högele, M. Kroner, S. Seidl, K. Karrai, M. Atatüre, J. Dreiser, A. Imamoglu, R. J. Warburton, A. Badolato, B. D. Gerardot, and P. M. Petroff, Spin-selective optical absorption of singly charged excitons in a quantum dot, *Appl. Phys. Lett.* **86**, 221905 (2005).
- [21] M. Kroner, S. Remi, A. Högele, S. Seidl, A. W. Holleitner, R. J. Warburton, B. D. Gerardot, P. M. Petroff, and K. Karrai, Resonant saturation laser spectroscopy of a single self-assembled quantum dot, *Physica (Amsterdam)* **40E**, 1994 (2008).
- [22] J. Dreiser, M. Atatüre, C. Galland, T. Müller, A. Badolato, and A. Imamoglu, Optical investigations of quantum dot spin dynamics as a function of external electric and magnetic fields, *Phys. Rev. B* **77**, 075317 (2008).
- [23] M. Kroner, K. M. Weiss, B. Biedermann, S. Seidl, S. Manus, A. W. Holleitner, A. Badolato, P. M. Petroff, B. D. Gerardot, R. J. Warburton, and K. Karrai, Optical detection of single-electron spin resonance in a quantum dot, *Phys. Rev. Lett.* **100**, 156803 (2008).
- [24] This performance can be compared to a precision of  $< 1\%$  obtained for measurement times of 10 s of a state-of-the-art SQUID-based thermometer reported by J. Beyer, M. Schmidt, J. Engert, S. AliValiollahi, and H. J. Barthelmeß, Reference measurements of SQUID-based magnetic-field fluctuation thermometers, *Supercond. Sci. Technol.* **26**, 065010 (2013).
- [25] A. V. Kuhlmann, J. Houel, D. Brunner, A. Ludwig, D. Reuter, A. D. Wieck, and R. J. Warburton, A dark-field microscope for background-free detection of resonance fluorescence from single semiconductor quantum dots operating in a set-and-forget mode, *Rev. Sci. Instrum.* **84**, 073905 (2013).
- [26] D. Maradan, L. Casparis, T.-M. Liu, D. E. F. Biesinger, C. P. Scheller, D. M. Zumbühl, J. D. Zimmerman, and A. C. Gossard, GaAs quantum dot thermometry using direct transport and charge sensing, *J. Low Temp. Phys.* **175**, 784 (2014).
- [27] M. Atatüre, J. Dreiser, A. Badolato, A. Högele, K. Karrai, and A. Imamoglu, Quantum-dot spin-state preparation with near-unity fidelity, *Science* **312**, 551 (2006).
- [28] J. M. Smith, P. A. Dalgarno, R. J. Warburton, A. O. Govorov, K. Karrai, B. D. Gerardot, and P. M. Petroff, Voltage control of the spin dynamics of an exciton in a semiconductor quantum dot, *Phys. Rev. Lett.* **94**, 197402 (2005).
- [29] S. Seidl, M. Kroner, P. A. Dalgarno, A. Högele, J. M. Smith, M. Ediger, B. D. Gerardot, J. M. Garcia, P. M. Petroff, K. Karrai, and R. J. Warburton, Absorption and photoluminescence spectroscopy on a single self-assembled charge-tunable quantum dot, *Phys. Rev. B* **72**, 195339 (2005).
- [30] J. Houel, A. V. Kuhlmann, L. Greuter, F. Xue, M. Poggio, B. D. Gerardot, P. A. Dalgarno, A. Badolato, P. M. Petroff, A. Ludwig, D. Reuter, A. D. Wieck, and R. J. Warburton, Probing single-charge fluctuations at a GaAs/AlAs interface using laser spectroscopy on a nearby InGaAs quantum dot, *Phys. Rev. Lett.* **108**, 107401 (2012).
- [31] C. Latta, A. Srivastava, and A. Imamoglu, Hyperfine interaction-dominated dynamics of nuclear spins in self-assembled InGaAs quantum dots, *Phys. Rev. Lett.* **107**, 167401 (2011).
- [32] C. Latta, A. Högele, Y. Zhao, A. N. Vamivakas, P. Maletinsky, M. Kroner, J. Dreiser, I. Carusotto, A. Badolato, D. Schuh, W. Wegscheider, M. Atatüre, and A. Imamoglu, Confluence of resonant laser excitation and bidirectional

- quantum-dot nuclear-spin polarization, *Nat. Phys.* **5**, 758 (2009).
- [33] A. Högele, M. Kroner, C. Latta, M. Claassen, I. Carusotto, C. Bulutay, and A. Imamoglu, Dynamic nuclear spin polarization in the resonant laser excitation of an InGaAs quantum dot, *Phys. Rev. Lett.* **108**, 197403 (2012).
- [34] X. Xu, Y. Wu, B. Sun, Q. Huang, J. Cheng, D. G. Steel, A. S. Bracker, D. Gammon, C. Emary, and L. J. Sham, Fast spin state initialization in a singly charged InAs-GaAs quantum dot by optical cooling, *Phys. Rev. Lett.* **99**, 097401 (2007).
- [35] D. Keller, D. R. Yakovlev, B. König, W. Ossau, Th. Gruber, A. Waag, L. W. Molenkamp, and A. V. Scherbakov, Heating of the magnetic ion system in (Zn, Mn)Se/(Zn, Be)Se semimagnetic quantum wells by means of photoexcitation, *Phys. Rev. B* **65**, 035313 (2001).
- [36] A. V. Koudinov, Yu. G. Kusrayev, and I. G. Aksyanov, Light-induced heating effects in semimagnetic quantum wells, *Phys. Rev. B* **68**, 085315 (2003).
- [37] The slightly larger temperature compared to other measurements presented here arises from a larger laser power that is used in this experiment.
- [38] B. Sviderski, M. Hanl, A. Weichselbaum, H. E. Türeci, M. Goldstein, L. I. Glazman, J. von Delft, and A. Imamoglu, Proposed Rabi-Kondo correlated state in a laser-driven semiconductor quantum dot, *Phys. Rev. Lett.* **111**, 157402 (2013).
- [39] B. R. Mollow, Power spectrum of light scattered by two-level systems, *Phys. Rev.* **188**, 1969 (1969).
- [40] A. Müller, W. Fang, J. Lawall, and G. S. Solomon, Emission spectrum of a dressed exciton-biexciton complex in a semiconductor quantum dot, *Phys. Rev. Lett.* **101**, 027401 (2008).
- [41] A. N. Vamivakas, M. Atatüre, J. Dreiser, S. T. Yilmaz, A. Badolato, A. K. Swan, B. B. Goldberg, A. Imamoglu, and M. S. Ünlü, Strong extinction of a far-field laser beam by a single quantum dot, *Nano Lett.* **7**, 2892 (2007).
- [42] M. P. Bakker, A. V. Barve, A. Zhan, L. A. Coldren, M. P. van Exter, and D. Bouwmeester, Polarization degenerate micropillars fabricated by designing elliptical oxide apertures, *Appl. Phys. Lett.* **104**, 151109 (2014).
- [43] F. Seilmeier, M. Hauck, E. Schubert, G. J. Schinner, S. E. Beavan, and A. Högele, following paper, Optical thermometry of an electron reservoir coupled to a self-assembled (In,Ga)As quantum dot below 1 K, *Phys. Rev. Applied* **2**, 024002 (2014).